RESEARCH ARTICLE
PLANETARY SCIENCE

Earth and Planetary Physics
2: 384–397, 2018
doi: 10.26464/epp2018036

Petrogenesis of basaltic shergottite NWA 8656

Ting Cao, Qi He*, and ZhuQing Xue

Planetary Science Institute, School of Earth Sciences, China University of Geosciences, Wuhan 430074, China

Abstract: Most basaltic shergottites are too Mg-rich to represent parent melt compositions because they contain some cumulus pyroxenes. However, basaltic shergottite Northwest Africa (NWA) 8656 with subophitic texture can be used as the parent melt composition in petrogenetic studies because it contains no or rare cumulus pyroxenes. Its pyroxene cores (Mg# 66-68, the most magnesian) are in equilibrium with the bulk rock composition based on major (Fe-Mg) and trace elements (REE—rare earth elements). The patchy zoning of pyroxenes has been interpreted as reflecting a two-stage crystallization history: 1) crystallization of Mg-rich pyroxene cores at depth (50 km, the base of Martian crust), 2) crystallization of Fe-rich pyroxene rims at the shallow depth near the Martian surface with a fast cooling history. The crystallization of Fe-rich pyroxenes and the existence of different symplectites indicate that NWA 8656 underwent eruption. The oxygen fugacity of NWA 8656 (QFM –0.9±0.5) suggests an oxidized condition at the late-stage crystallization process, and the CI-normalized REE patterns of different minerals show enrichment in LREE, compared to that of depleted shergottites. Both of these observations suggest a relatively ITE (incompatible trace elements)-enriched signature of NWA 8656, similar to those of other enriched shergottites. The REE compositions of augite core and rim and plagioclase can be successfully reproduced by progressive crystallization without exogenous components, which indicates a closed magmatic system for NWA 8656. Consequently, we conclude that the ITE-enriched signature of NWA 8656 is inherited from an enriched mantle source rather than caused by crustal assimilation. Moreover, partial melting of depleted Martian mantle could not directly yield magmas that have geochemical characteristics similar to enriched shergottite parent magmas, so the enriched and depleted shergottites are derived from distinct mantle sources, and the mantle source of enriched shergottites would be expected to contain ilmenite.

Keywords: basaltic shergottites; patchy zoning; ITE-enriched; closed-system; distinct mantle sources

Citation: Cao T., He Q., and Xue Z. Q. (2018). Petrogenesis of basaltic shergottite NWA 8656. *Earth Planet. Phys.*, *2*(5), 384–397. http://doi.org/10.26464/epp2018036

1. Introduction

Shergottites act as the youngest and most common Martian meteorites, providing significant constraints on Martian magmatic processes and history. Texturally, shergottites have been divided into three subgroups: basaltic, olivine-phyric, and lherzolitic (Bridges and Warren, 2006; Goodrich, 2002; McSween and Treiman, 1998). Most basaltic shergottites are described as subophitic, dominated by zoning pyroxenes and maskelynite (shock-induced glassy plagioclase). But some basaltic shergottites are too Mg-rich to represent parent melt compositions because they contain some cumulus pyroxenes (e.g. Filiberto et al., 2010; Goodrich, 2003).

Geochemically, shergottites also have been divided into three subgroups: enriched, intermediate, and depleted (Bridges and Warren, 2006; Papike et al., 2009; Shearer et al., 2013; Symes et al., 2008), which present huge differences in major and trace element compositions, isotopic compositions, and crystallization ages (Borg et al., 1997; Bouvier et al., 2008a, b ; Jones, 1986; Lodders, 1998; Nyquist et al., 1995, 2001; Shih et al., 1982, 2003). The depleted shergottites are mantle-derived origin and formed by partial melting of depleted Martian mantle (Borg and Draper, 2003). However, enriched shergottites are attributed to 1) varying degrees of assimilation of enriched Martian crust (Blichert-Tolt et al., 1999; Herd et al., 2002; Wadhwa, 2001), or 2) heterogeneity of Martian mantle sources. The enriched mantle source is associated with late-stage residual melts formed after high solidification of the primitive Martian magma ocean (Borg and Draper, 2003; Debaille et al., 2007, 2008).

However, a growing body of evidence against the view that the ITE-enriched signature of shergottites is caused by Martian crustal assimilation (Brandon et al., 2012; Ferdous et al., 2017; Shafer et al., 2010). For instance, the mixing and assimilation-fractional crystallization (AFC) model, using depleted shergottites and Martian crust as end-members, can reproduce geochemical characteristics similar to the intermediate and enriched shergottites, based on REE and Sr/Nd isotopic compositions (Ferdous et al., 2017; Shih et al., 2003; Warren and Bridges, 2005). But it fails to explain: 1) Os and Nd isotopic systematics of shergottites (Brandon et al., 2012); 2) the correlation between major element (Mg#) and trace element ratios (e.g. Sm/Eu) or isotopes (e.g. ε_{Nd}); and 3) the huge range of major elements in enriched shergottites. Moreover, the REE abundances in different minerals of most enriched shergottites are consistent with a history of progressive crystallization, for

Correspondence to: Q. He, he_qi@cug.edu.cn
Received 05 AUG 2018; Accepted 27 SEP 2018.
Accepted article online 28 SEP 2018.

example NWA 856 and LAR 06319, which suggests a closed magmatic system without geochemical disturbance from crustal assimilation (Ferdous et al., 2017; Shafer et al., 2010). Based on the above discussion, we embrace the idea of heterogeneity of Martian mantle sources.

In order to ascertain the origin of the ITE-enriched signature in shergottites, we have chosen to study the enriched shergottites of NWA 8656. NWA 8656 was found in Algeria in 2014; its total weight was 1656 g. Previous study reported NWA 8656's petrology and mineralogy characteristics, which suggest that it is basaltic shergottite with subophitic texture. In this paper, we investigate whether NWA 8656 could represent the parent melt composition, based on the bulk rock composition of NWA 8657 (paired with NWA 8656, Howarth et al., 2017) and we further study the origin of the enriched signature of NWA 8656.

2. Analytical Methods

Two polished thick sections (one inch in size) of NWA 8656 were prepared and examined to study their petrographic and mineralogical characteristics. Backscattered electron (BSE) images were taken with Quanta 200 and Quanta 450 FEG scanning electron microscopes with energy dispersive spectrometer (EDS) at the State Key Laboratory of Geological Processes and Mineral Resources, China University of Geosciences, Wuhan. The modal abundance of each phase in the thick section was estimated from pixel points counted on mosaic bulk-rock BSE images by Photoshop. Various element distribution maps (Mg, Ca, Fe) can be used to better analyze the complex chemical zoning of pyroxenes.

Major element quantitative analysis of most silicate and Fe-Ti oxide minerals was measured by a JEOL JXA 8100 electron microprobe (EMP) at China University of Geosciences, Wuhan, and a JXA-8230 at Wuhan University of Technology. The reference minerals are natural and synthetic minerals (albite-Na, olivine-Mg, anorthite-Al, apatite-P, orthoclase-K, wollastonite-Si+Ca, rutile-Ti, chromite-Cr, rhodonite -Mn, hematite-Fe). Spot analysis was done with 15 kV accelerating voltage, 20 nA beam current, and 1 μm beam size, except 10 nA beam current and 5 μm beam size for phosphates, maskelynite, and glassy phase in order to avoid the loss of Na and K. Counting time is 20 s for both peak and background. Detection limits (3σ above background) are typically 0.03 wt% for SiO_2, TiO_2, Al_2O_3, Cr_2O_3, MgO, MnO and CaO, and 0.05 wt% for FeO, Na_2O, and K_2O. Results of representative microprobe analyses are shown in Tables 1 and 2.

In situ trace element analyses of pyroxenes, maskelynite, and phosphates were determined by an Agilent 7500a inductively coupled plasma mass spectrometry coupled with a GeoLas 2005 laser ablation system (LA-ICP-MS) at the State Key Laboratory of Geological Processes and Mineral Resources, China University of Geosciences, Wuhan. All mineral phases were analyzed with a 44 μm beam spot. Each analysis included an approximately 20 s background acquisition (gas blank) and 50 s data acquisition for the sample. Software ICPMSDataCal was used to carry out off-line selection and integration of background and analyte signals, and time-drift correction and quantitative calibration. The USGS reference glasses (BCR-2G, BHVO-2G, and BIR-1G) were used as reference materials for external calibration and major element compositions of pyroxenes, maskelynite, and phosphates were used as internal standards (MgO for pyroxenes, CaO for maskelynite and phosphates). In addition, NBS 610 was analyzed with 8 sample spot intervals in order to correct the time-dependent drift of sensitivity and mass discrimination. More specific details about operating conditions and data reduction are described by Liu YS et al. (2008) and Chen L et al. (2011). Representative trace element analyses are shown in Table 3.

3. Petrography and Mineral Chemistry

The exterior of NWA 8656 is free of evident fusion crust. Its interior shows a dominantly medium-grained subophitic texture that consists of elongated prismatic pyroxene (up to 2.5 mm in length) and lath-like maskelynite (up to 1.3 mm in length). Crystal size distribution studies have shown that basaltic shergottites should include "coarse-grained" pyroxene and maskelynite set in a "fine-grained" groundmass (Lentz and McSween, 2000). However, similar to NWA 6939 (Filiberto et al., 2014), NWA 8656 mostly consists of medium-grained pyroxene and maskelynite (Figure 1a) rather than a fine-grained groundmass and coarse-grained phenocryst. Modal proportions of minerals are 64.9 vol% for pyroxene, 31.4 vol% for maskelynite, 2.2 vol% for Fe-Ti oxides, and 1 vol% for phosphates, and trace amounts of mesostasis. The presence of shock-induced melt pockets and maskelynite indicate that the parent rock experienced strong shock metamorphism.

Pyroxenes are the predominant phases of NWA 8656 and occur as euhedral to subhedral, elongated prismatic grains, 1–2.5 mm in length (average grain size is ~1.8 mm) (Figure 1a). Pyroxenes show patchy zoning from Mg-rich cores to Mg-poor rims. Pyroxene cores are augite ($En_{42}Wo_{38}$ to $En_{25}Wo_{32}$) or pigeonite ($En_{55}Wo_{12}$ to $En_{27}Wo_{17}$) without intermediate composition of Wo. Pyroxene rims with progressive enrichment of Fe ($En_{19}Wo_{25}$-$En_{23}Wo_{13}$) vary greatly in Ca content (Figure 2a, Table 1). These Fe-rich compositions plot almost in the "forbidden zone" and have been described as metastable pyroxene. Although the contrast between the cores and the rims is obvious in BSE images, it is hard to directly distinguish augite from pigeonite for Mg-rich cores. So X-ray maps of different elements (Mg, Ca, Fe) can be used to distinguish augite from pigeonite. The Mg-rich augite and pigeonite mostly occur as pyroxene cores; however, Mg-rich pigeonite also occurs as patches with irregular boundaries (Figure 1b). The extreme Fe-rich pyroxenes appear as rims of both augite and pigeonite, though some are very small (Figures 1b and 1c). Rare pyroxferroite ($Fs_{87}Wo_5$) grains can be found in mesostasis (Figure 2a).

Compared to the Fe-rich rims, the composition of early-formed pyroxenes (Mg# 60–68) are homogeneous without zoning, which is similar to Shergotty and EETA 79001B (Figure 2a); this homogeneity is caused by subsolidus redistribution and reequilibration of Fe-Mg (Treiman, 1996). The reequilibration also can be reflected in the variation of Ti, which is homogeneous within most magnesian pyroxene cores but varies greatly for pyroxene rims (Figure 2c). The minor elements also show a correlation from pyroxene cores to rims. The abundance of Ti is negatively correlated with that of Mg#, whereas the correlation with Al is the re-

Table 1. Representative electron microprobe analyses (EMP) (in wt%) of pyroxenes and Fe-Ti oxides in NWA 8656

Phase	Pyroxene					Fe-Ti oxides			
	Core		Rim						
	Aug-core	Pig-core	Aug	Pig	Fe-rich		Ilm		TMt
SiO_2	51.90	52.14	48.54	48.69	48.15	SiO_2	0.24		0.10
CaO	18.17	7.34	13.11	5.89	10.92	CaO	—		—
TiO_2	0.25	0.20	0.60	0.46	0.59	TiO_2	51.71		27.51
FeO	11.93	18.98	29.21	35.95	31.79	FeO	46.46		68.16
MgO	14.15	18.24	6.26	7.26	6.02	MgO	0.45		0.31
Al_2O_3	1.32	0.90	0.73	0.42	0.67	Al_2O_3	0.13		1.30
MnO	0.43	0.68	0.71	0.89	0.79	MnO	0.62		0.55
Na_2O	0.17	0.08	0.10	0.03	0.12	Na_2O	—		0.00
K_2O	—	—	0.01	—	—	K_2O	—		0.01
Cr_2O_3	0.61	0.52	0.03	0.01	0.01	Cr_2O_3	0.10		0.37
P_2O_5	—	—	—	—	—	P_2O_5	—		—
SO_3	—	—	—	—	—	SO_3	—		—
Total	98.93	99.08	99.29	99.61	99.06	Total	99.72		98.31
O	6	6	6	6	6	O	3		4
Si	1.97	1.97	1.97	1.99	1.97	Si	0.01		—
Ca	0.74	0.30	0.57	0.26	0.48	Ca	—		—
Ti	0.01	0.01	0.02	0.01	0.02	Ti	0.98		0.81
Fe^{2+}	0.10	0.16	0.26	0.57	0.50	Fe^{2+}	0.94		1.64
Fe^{3+}	0.28	0.44	0.73	0.65	0.51	Fe^{3+}	0.04		0.59
Mg	0.80	1.04	0.38	0.45	0.37	Mg	0.02		0.02
Al	0.06	0.04	0.03	0.02	0.03	Al	—		0.06
Mn	0.01	0.02	0.02	0.03	0.03	Mn	0.01		0.02
Na	0.01	0.01	0.01	—	0.01	Na	—		—
K	—	—	—	—	—	K	—		—
Cr	0.02	0.02	—	—	—	Cr	0.00		0.01
Total	3.99	4.00	4.00	3.99	4.00	Total	2.01		3.15
Mg#	68.11	63.36	27.82	26.67	25.41	Ilm	93.01	Mt	23.17
Fs	19.60	30.99	50.96	63.52	56.10	Hm	3.97	Usp	73.36
En	41.90	53.59	19.64	23.10	19.11	Py	1.32	Sp	2.91
Wo	38.40	15.41	29.40	13.38	24.78	Gk	1.70	Chr	0.56

Notes: Aug = augite; Pgt = pigeonite; Fe-rich = extreme Fe-rich pigeonite; Ilm = ilmenite; Mg# = Mg/(Mg+Fe^T), using afu; the mol of Fe^{3+} and Fe^{2+} is determined by residual oxygen calculation, Ox= total theoretical anion – total calculated anion, Fe^{3+}=2×Ox, Fe^{2+}=(FeO wt%-0.9×160×Ox)/72; Usp (Fe_2TiO_4) = molar 100×2Ti/[2Ti + Cr + Al + Fe^{3+}]; Mt ($FeFe_2O_4$) = molar 100×Fe^{3+}/[2Ti + Cr + Al+Fe^{3+}]; Chr ($FeCr_2O_4$) = molar 100×Cr/[2Ti + Cr + Al + Fe^{3+}]; Sp ($MgAl_2O_4$) = molar 100×Al/[2Ti + Cr + Al + Fe^{3+}]; defined in Goodrich (2003) ; the calculation of Ilm ($FeTiO_3$), Hm (Fe_2O_3), Py ($MnTiO_3$) and Gy ($MgTiO_3$) referred to Ghiorso and Sack (1991).

verse; the abundance of Ti increases with increasing Al for pyroxene cores, while for rims Ti increases as Al decreases (Figure 2b).

Plagioclase is subhedral lath-shaped and interstitial to pyroxene with lengths 0.8–1.3 mm. However, plagioclase has been completely converted into maskelynite because of shock metamorphism. Plagioclase is characterized by relatively homogeneous composition ranging from $An_{49}Or_1$ to $An_{52}Or_7$ (Table 2) and a few of them are enriched in K ($An_{45}Or_{17}$, NaO+K_2O up to 5 wt %). In addition, feldspathic glass (SiO_2 66–85%) and nearly pure silica glass (SiO_2 ~95%) always occur in the late-stage assemblage with sharp edges and corners in maskelynite, coupled with a few fine-grained metallic minerals, e.g. troilite.

Table 2. Representative electron microprobe analyses (EMP) (in wt%) of maskelynite, glass and phosphates in NWA 8656

Phase	Maskelynite		Glass				Phosphates		
		K-rich	Q	K-Gl	Gl	Fa	Phase	Mer	Ap
SiO_2	55.00	57.29	95.23	74.64	85.45	30.66	Na_2O	1.17	0.15
CaO	12.04	9.37	0.37	3.01	2.40	1.77	SiO_2	0.03	1.74
TiO_2	0.02	0.03	0.27	0.12	0.19	0.20	TiO_2	0.00	0.12
FeO	0.85	0.59	0.08	0.90	0.36	63.23	CaO	47.14	53.69
MgO	0.09	0.05	0.02	0.01	0.02	0.70	P_2O_5	46.00	40.79
Al_2O_3	26.79	25.75	2.38	15.72	9.07	0.27	FeO	4.21	2.17
MnO	0.05	0.00	0.02	0.00	0.04	1.55	MgO	1.35	0.02
Na_2O	4.77	4.20	0.48	1.65	1.10	0.04	Al_2O_3	0.04	0.19
K_2O	0.11	2.39	0.32	2.82	0.79	0.01	K_2O	0.01	2.04
Cr_2O_3	—	—	0.02	—	0.02	0.03	Cl	0.17	0.16
Total	99.73	99.65	99.20	98.89	99.42	98.45	F	0.00	1.33
O	8	8	—	—	—	4	Total	100.11	101.37
Si	2.50	2.60	—	—	—	1.03	—	—	—
Ca	0.59	0.46	—	—	—	0.06	—	—	—
Ti	—	—	—	—	—	0.00	—	—	—
Fe^T	0.03	0.02	—	—	—	1.77	—	—	—
Mg	0.01	—	—	—	—	0.04	—	—	—
Al	1.43	1.37	—	—	—	0.01	—	—	—
Mn	—	—	—	—	—	0.04	—	—	—
Na	0.42	0.37	—	—	—	—	—	—	—
K	0.01	0.14	—	—	—	—	—	—	—
Cr	—	—	—	—	—	—	—	—	—
Total	4.99	4.96	—	—	—	2.96	—	—	—
Or	0.61	14.37	—	—	—	—	—	—	—
An	57.91	47.31	—	—	—	—	—	—	—
Ab	41.47	38.32	—	—	—	—	—	—	—

Notes: Gl = glass; Q = SiO_2-rich glass; K-Gl = K-rich glass; Fa = fayalite; Ap = apatite.

Fe-Ti oxides appear as anhedral texture. Both titanomagnetite and ilmenite are observed in NWA 8656, located mostly in Fe-rich pyroxene rims with the composition of $Usp_{65\text{-}74}Mt_{23\text{-}30}Sp_{3\text{-}4}$ $Chr_{0\text{-}0.7}$ for titanomagnetite and $Ilm_{92\text{-}96}Hm_{1\text{-}5}Gk_{1\text{-}1.7}Py_{1\text{-}2}$ for ilmenite (Table 1). Widespread exsolution of ilmenite is observed in titanomagnetite grains. Some large titanomagnetite grains are encircled by 2–6 μm fayalite reaction rims (Figure 3b). Similar mineral assemblage also can be observed in other basaltic shergottites, e.g. NWA 2975 (He Q et al., 2015). The nearly pure silica glass formed by the late-stage residual melt also can be found in ulvospinel grains.

Other accessory minerals include phosphates, fayalite, troilite, and silica. The phosphates are merrillite and apatite. They are found close to the Fe-rich pyroxene rims with anhedral texture (Figure 1a). Other accessory minerals are always present as late-stage mineral assemblage, such as 1) Three-phase symplectites, pyroxene, and fayalite, that intergrow homogenously with Si-rich glass around the junction. This symplectites is always adjacent to Fe-rich pyroxenes and displays vermicular texture (Figure 3a); 2) Two-phase symplectite appears as an intergrowth of fayalite and Si-rich glass with fine-grained (1–2 μm) vermicular to micrographic texture. This symplectities is commonly close to thin fayalite rims of Fe-Ti oxides or occasionally close to phosphates (Figure 3b). Both types of symplectites are interpreted as breakdown products of rapidly cooling Fe-rich pyroxenes under low pressure (Aramovich et al., 2002; Patzer and McSween, 2012; Rost et al., 2009); 3) "Coarse-grained" (4–5 μm) multi-phase mineral assemblages are found, containing Fe-Ti oxides, phosphates, fayalite, Si-rich glass, Fe-rich pyroxenes (Figure 3c); 4) Si-rich and Si-Al-K-rich glass generally occurs as vesicular or micrographic assemblages invading in maskelynite, and the assemblages also contain very fine-grained metallic minerals, iron oxides, or sulfides (Figure 3d). Besides, nearly pure silica (SiO_2>95%) always occurs in pyroxenes,

Table 3. Representative trace element compositions (in ppm) of minerals in NWA 8656

ppm	SRM 610	1σ	d.l.	Pig-core	Aug-core	Pig rim	Mask	Mer
Sc	442	8.47	0.027	50.6	87.1	97.6	0.49	251
V	437	8.12	0.016	295	522	496	4.57	212
Cr	411	8.26	0.26	2553	3243	1652	—	170
Co	387	7.15	0.0102	50.7	34.4	50.2	0.82	106
Ni	437	7.68	0.13	154	104	81.2	0.88	82.8
Rb	395	6.78	0.041	0.15	0.21	0.12	1.01	756
Sr	522	11.0	0.0036	21.9	21.6	5.78	179	179
Y	467	9.48	—	2.87	5.76	7.81	0.09	352
Zr	458	8.78	0.036	2.17	4.82	5.35	0.31	3044
Ba	454	9.11	0.033	203	155	14.5	81.5	733
La	421	9.16	—	0.03	0.09	0.06	0.13	63.8
Ce	444	8.47	0.0028	0.13	0.38	0.43	0.26	150
Pr	444	8.48	0.0024	0.02	0.08	0.09	0.03	22.1
Nd	438	8.47	—	0.14	0.59	0.68	0.13	104
Sm	460	8.63	0.016	0.11	0.32	0.58	0.03	39.4
Eu	453	8.26	0.0050	0.04	0.13	0.15	0.58	12.1
Gd	442	8.57	0.016	0.24	0.70	1.11	0.04	54.6
Tb	436	8.38	0.0024	0.05	0.14	0.18	—	10.2
Dy	442	8.74	—	0.48	1.02	1.41	0.03	64.8
Ho	440	8.52	—	0.11	0.23	0.25	0.01	13.0
Er	460	8.78	0.0075	0.34	0.62	0.87	0.01	37.2
Tm	439	8.53	0.0035	0.05	0.09	0.12	—	4.90
Yb	456	9.06	0.016	0.42	0.60	0.93	0.01	30.1
Lu	445	8.72	—	0.05	0.08	0.13	—	4.00
Hf	424	8.05	—	0.09	0.21	0.34	0.01	75.3
Ta	472	8.97	—	—	—	0.01	—	3.54
Th	451	8.48	0.0053	—	—	—	—	10.4
U	439	8.70	—	0.01	0.01	—	—	3.07

Note: d.l. = detection limit.

Fe-Ti oxides, or phosphates.

3.1 Shock Metamorphism

Highly fractured pyroxenes, transformation of plagioclase into maskelynite, and abundant shock melt pockets all suggest that NWA 8656 underwent strong shock metamorphism. Maskelynite is a diagnostic feature for shergottites and it suggests a shock pressure of up to 40 GPa (Fritz et al., 2005). The large shock melt pocket contains unmelted maskelynite and pyroxene crystals that appear as rounded patches surrounded by resorbed margins and reaction coronas. Shock melt pockets arecommonly observed in most other basaltic shergottites. The presence of pyroxferroite in late-stage assemblage (Figure 3c) also suggests that the parent rock experienced a history of high pressure and fast cooling, because it is stable only at pressures $\geq$1.0 GPa (Lindsley and Burnham, 1970).

3.2 REE Composition

All pyroxenes display parallel LREE (light rare earth elements)-depleted patterns, but augite is slightly more enriched than pigeonite. Pyroxene rim is more enriched than core, $(La/Yb)_{CI}$ = 0.06 for Mg# 62–67 versus $(La/Yb)_{CI}$ = 0.1 for Mg# 45. These REE patterns are almost parallel to those of Shergotty (Wadhwa et al., 1994), though with slightly higher REE concentrations. The pyroxene rim also has a negative Eu anomaly (δEu_{rim}= 0.57, $\delta Eu= 2\times Eu_{CI}/[Sm_{CI} + Gd_{CI}]$, Figure 4a), suggesting a history of plagioclase crystallization. A few pigeonites have higher La values accompanied by a small negative Ce anomaly (δCe= 0.82, $\delta Ce= 2\times Ce_{CI}/[La_{CI} + Pr_{CI}]$, Figure 4b); this pattern is interpreted to be evidence of terrestrial weathering (Crozaz et al., 2003; Wadhwa et al., 1994).

On the contrary, patterns of plagioclase are characterized by LREE-enrichment with large positive Eu anomalies (δEu = 54–89, Figure

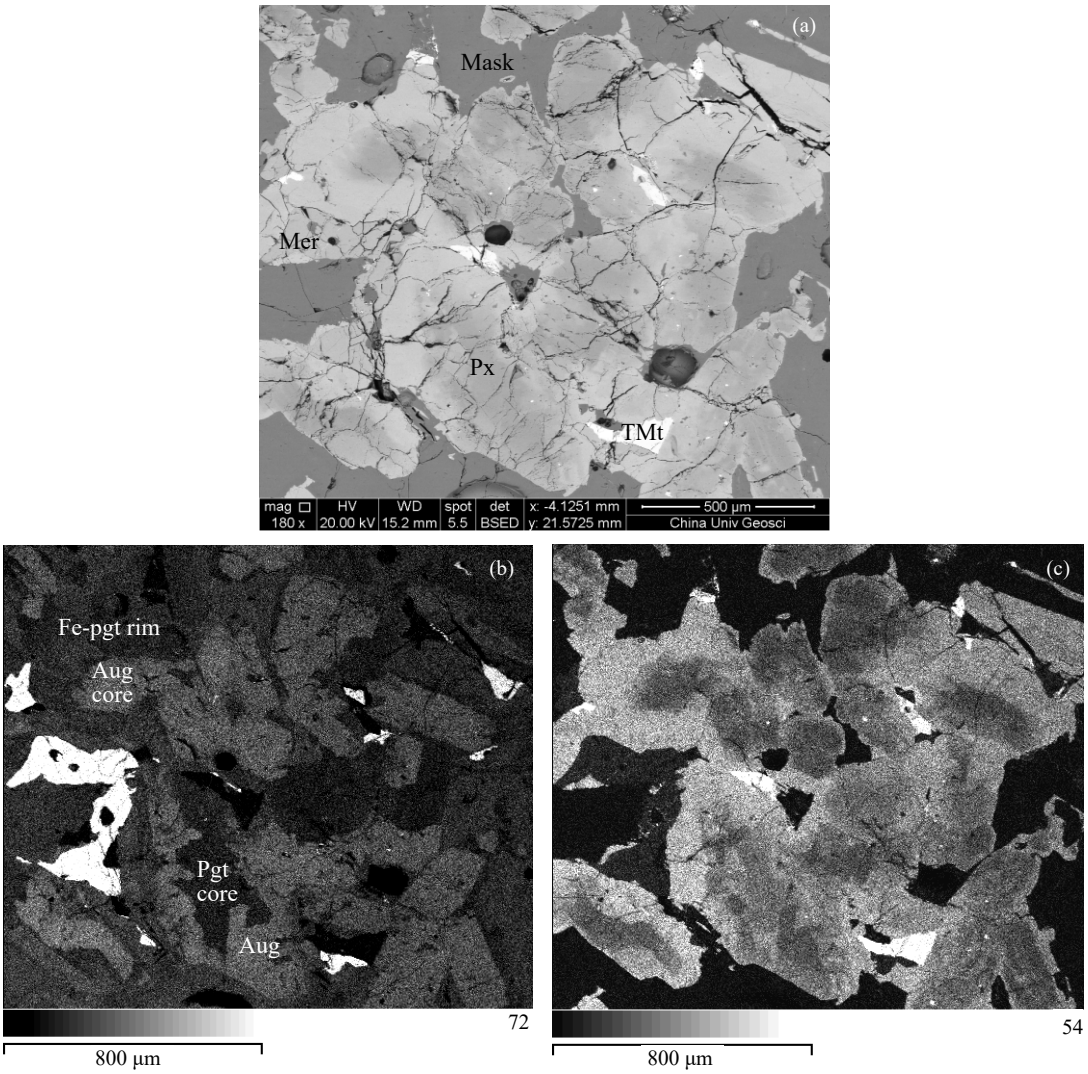

Figure 1. Backscatter electron (BSE) images of NWA 8656. (a) Image of the thick section shows a subophitic texture; (b) and (c) element distribution maps of Ca and Fe, respectively. Px = pyroxene, Mask = maskelynite, TMt = titanomagnetite, Mer = merrillite, Aug= augite, Pgt=pigeonite, Fe-pgt=Fe-rich pigeonite.

4c), which is similar to Shergotty (Wadhwa et al., 1994). Abundances of HREE (heavy rare earth elements) in plagioclase are much lower than LREE [$(La/Yb)_{CI}$ = 8–9], not only because they are relatively low, but also because of molecular interferences from the LREE oxides in the HREE mass region. As is the case for most basaltic shergottites, the merrillite of NWA 8656 is its main REE carrier, with REE concentrations two orders of magnitude higher than in other phases. This merrillite has a flat REE pattern [$(La/Yb)_{CI}$ = 1.5] with a small negative Eu anomaly [(δEu = 0.8)] (Table 3, Figure 4d). The concentrations of REE in merrillite are lower than in Shergotty; however, the abundance of maskelynite is identical to that of Shergotty. This difference is ascribed to the heterogeneous distribution of merrillite in NWA 8656. Based on the above descriptions, REE patterns or concentrations of all these minerals are in agreement with enriched shergottites, like Shergotty, and distinct from depleted and intermediated shergottites, such as QUE94201 and EETA 79001 (Lundberg et al., 1988, 1990; Wadhwa et al., 1994).

4. Discussion

4.1 Crystallization Conditions

The crystallization temperature of NWA 8656 can be calculated by two-pyroxene thermometry from Lindsley and Andersen (1983). Two approaches are available: 1) the compositions of most primitive pyroxene pairs (augite-pigeonite, Mg#>55) would be projected to the quadrilateral pyroxene thermometer and then acquire a crystallization temperature of 1020–1230 ± 30 °C; 2) 1200–1260 °C is a consolute temperature for augite + pigeonite cores estimated by an index of differentiation [*X*=Fe/(Mg + Fe), 0.32–0.4]; this value is consistent with the temperature of 1).

Ti/Al ratios in pyroxenes also provide a constraint on crystallization pressure in magmatic evolution by their systematic variation along with the degree of differentiation. A Ti/Al barometer for Martian samples that was calibrated by Filiberto et al. (2010) has been used to assess the crystallization pressure for NWA 8656. As Figure 2b shows, the low Ti/Al ratios of pyroxene cores are consistent with a crystallization pressure of 9.3 kbar, corresponding to

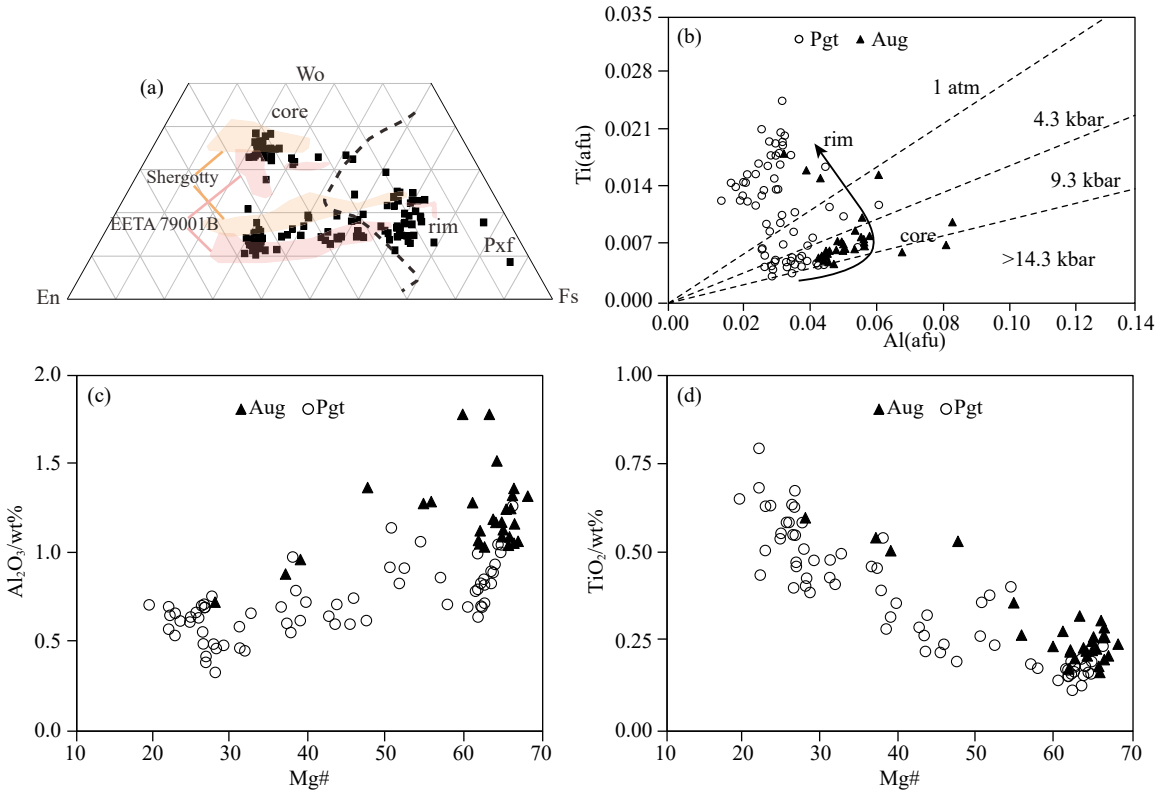

Figure 2. Pyroxene compositions in NWA 8656. (a) The quadrilateral plot of pyroxene compositions. The dashed line represents the pyroxene "forbidden region" in which pyroxene is not stable at low pressure (Lindsley, 1983). Yellow and pink areas outline the pyroxene compositions of Shergotty (Stöffler et al. 1986) and EETA 79001B (Mikouchi et al., 1999) from core to rim in order to compare with NWA 8656; (b) Ti-Al systematics of pyroxenes in NWA 8656, Al (afu) versus Ti (afu) with experimental fields for crystallization pressure, from Filiberto et al. (2010); (c) and (d) Covariations of Al_2O_3 and Ti_2O (wt %) with Mg# in pyroxenes. Pxf = pyroxferroite.

a depth of 50 km on Mars, equivalent to the base of the Martian crust or the boundary of mantle and crust (Wieczoreck and Zuber, 2004); the high Ti/Al ratios of pyroxene rims are consistent with a low pressure of < 0.1 MPa, indicating crystallization on the Martian surface.

The Fe-Ti oxide geothermometer/oxygen barometer developed by Ghiorso (Ghiorso and Evans, 1991; Ghiorso and Sack, 2008) is used to estimate oxygen fugacity (fO_2). The Fe/Ti exchange between co-existing ilmenite and titanomagnetite pairs was used to determine the closure temperature and fO_2. The oxygen fugacity and the equilibrium temperature of NWA 8656 parent melt are determined to be QFM (quartz–fayalite–magnetite) –0.9±0.5 and 800–880 °C for late-stage crystallization process. Moreover, the intergrowth of fayalite and silica (two-phase symplectite) in NWA 8656 also suggests an oxygen fugacity close to FMQ buffer in the late-stage crystallization process, which is also consistent with the estimated fO_2 value. Although the oxygen fugacity recorded by Fe-Ti oxides can represent only the late-stage oxidation state of the crystallization process, the oxygen fugacity of NWA 8656 is similar to that of the enriched shergottite suite (Herd, 2006; Herd et al., 2001, 2002), e.g. QFM –1.17 for Shergotty, QFM –1.22 for Zagami, QFM –1.33 for Los Angeles, and is much higher than that in depleted shergottites, QFM –3.01 for QUE94201, which were also estimated by the Ghiorso-Sack model. Hence, the oxygen fugacity of NWA 8656 suggests an oxidized late-stage crystallization condition that is similar to what is found in other enriched shergottites.

4.2 Crystallization Sequence

Besides petrologic texture, the covariation of Al/Ti and the index of differentiation (such as Mg#) in pyroxenes is used to infer the crystallization history. This approach has been extensively applied to lunar and Martian basalt (e.g. Anand et al., 2006; Udry et al., 2017). Hence, the crystallization history of NWA 8656 can be inferred from the record of compositional zoning of pyroxene. As Figure 2 shows, augite and pigeonite cores have similar Mg# ($Mg\#_{pgt}$= 65, $Mg\#_{aug}$= 68), so they appear as the earliest phases and crystallized almost simultaneously. This is consistent with Shergotty and Zagami (McSween, 1994; Stöffler et al., 1986,), but different from QUE 94201 and NWA 480, in which the earliest phase is pigeonite, which then was mantled by augite (Barrat et al., 2002; Mikouchi et al., 1999). Texturally, Fe-rich pyroxenes occur as pyroxene rims, indicating that they crystallized after Mg-rich pigeonite and augite. Substantial previous research has shown that the pyroxenes in shergottites formed prior to plagioclase (e.g. McSween, 1994; Hui HJ et al., 2011); these studies conclude that the covariation trend of Al/Ti in pyroxenes is closely associated with the crystallization of plagioclase. As Figure 2b shows, Ti increases along with Al for pyroxene cores, while Ti increases along with decreasing Al for pyroxene rims, this pattern attributed to the crystallization of plagioclase and the crystalliza-

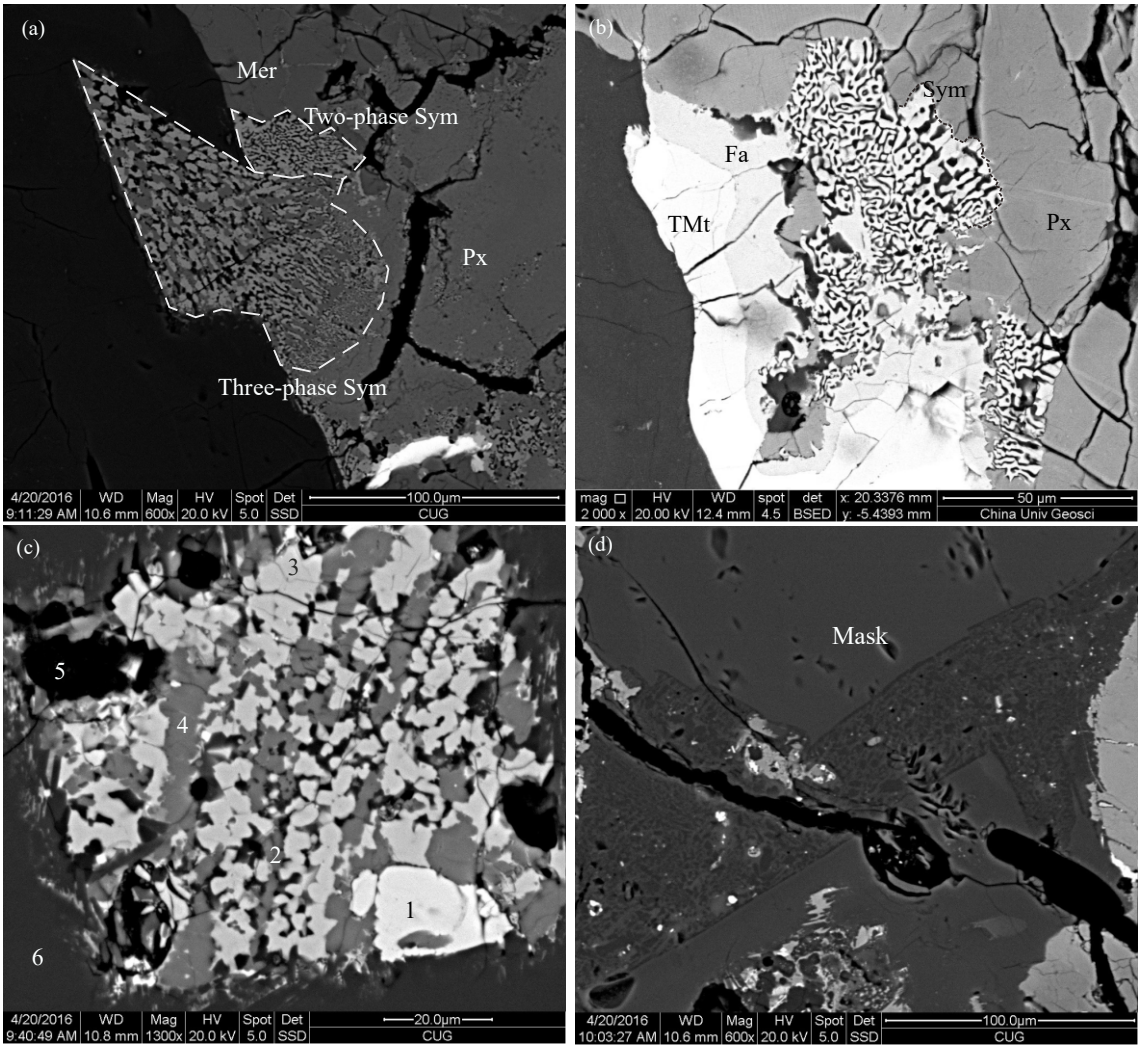

Figure 3. Petrographic features of late-stage mineral assemblage. (a) A three-phase symplectite adjacent to Fe-rich pyroxene and translated to two-phase vermicular symplectite adjacent to merrillite; (b) A two-phase vermicular symplectite adjacent to fayalite reaction rim; (c) A multi-phase assemblage in maskelynite (6), composed of 1. Fe-Ti oxides, 2. pyroxferroite, 3.fayalite, 4. phosphate, 5. glass; (d) Extremely Si-rich (dark) and Si -Al-K-rich glass (light gray) occurs as a late-stage assemblage.

tion of Mg-rich pyroxenes (Mg# 60–68) followed by plagioclase. Texturally, it is conspicuous to deduce that Fe-Ti oxides and phosphates with anhedraltexture appear as late-stage crystallization phases (Figure 3). In addition, the negative Eu anomaly in pyroxene rims and merrillite also suggests that they crystallized after plagioclase.

Augite is mostly surrounded by Fe-rich pigeonite in NWA 8656, which indicates that only low-Ca pyroxenes crystallize in the late-stages of the crystallization process. Moreover, all the phosphates occur in Fe-rich pyroxene rims, so the formation of phosphates implies a great deal of depletion of Ca and a lower concentration of Ca in residual melts for late-stage pyroxene crystallization. So it is evident to assume that the suppression of high-Ca pyroxene crystallization in the late-stage is associated with the formation of phosphates, despite the small amount of phosphate observed. The decrease of Ca in late-stage crystallization of pyroxenes is also interpreted by McSween et al. (1996) and Barrat et al. (2002) to be a result of co-crystallization of plagioclase. Consequently, the crystallization history of NWA 8656 appears to be: Mg-rich pyroxenes – plagioclase – Fe-rich pyroxenes – phosphates and Fe-Ti oxides (titanomagnetite).

4.3 Magma Evolution

The complex chemical zoning of pyroxenes indicates changing crystallization conditions during the crystallization process. The Fe-rich pyroxenes ($En_{30\text{-}15}Wo_{13\text{-}25}$) show various compositions of Ca, whereas this variation is absent in Mg-rich pyroxenes ($En_{42\text{-}25}Wo_{38\text{-}32}$, $En_{55\text{-}27}Wo_{12\text{-}17}$). Furthermore, these Fe-rich pyroxenes almost plot in the “forbidden zone”, indicating that they are metastable solid phases. Hence, the early-stage pyroxenes had enough time to crystallize slowly and produced a homogeneous Ca composition. In contrast, the late-stage Fe-rich pyroxenes might not have enough time to crystallize slowly and experience subsolidus re-equilibration, thus presenting heterogeneous Ca composition.

Additionally, the patchy zoning and irregular boundaries of pyroxene cores in NWA 8656 are interpreted as evidence of magma eruption; patchy zonings and irregular boundaries are ex-

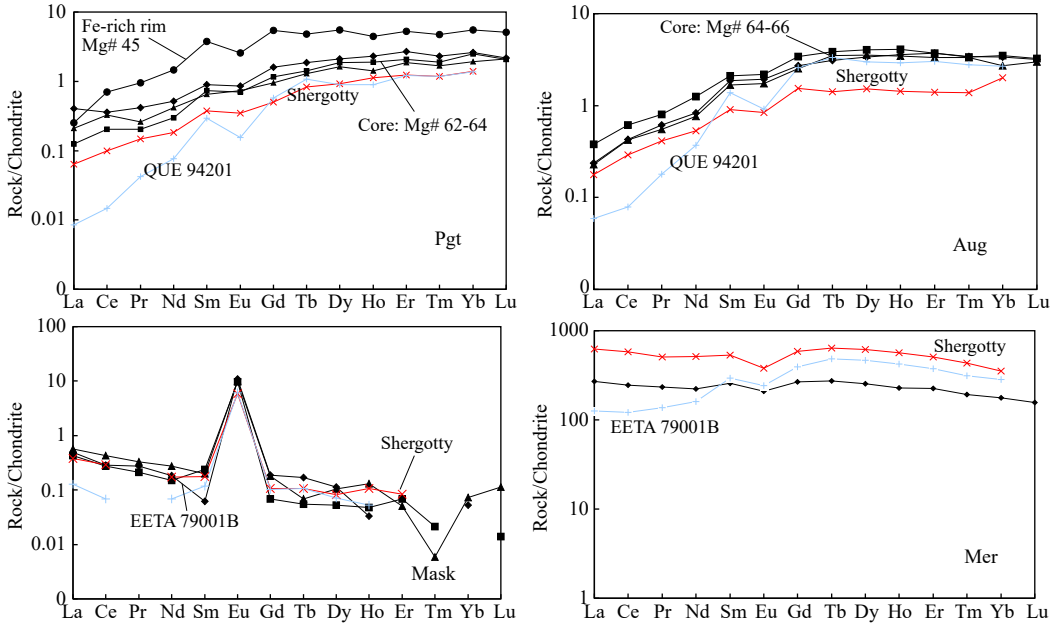

Figure 4. REE concentrations of pyroxenes, maskelynite, and merrillite of NWA 8656, Shergotty, EETA 79001B (Wadhwa et al., 1994), and QUE 94201 (McSween et al., 1996). All the elements are normalized to CI chondrite values (Sun and McDonough, 1989).

plained as dissolution and resorption of pyroxene cores during magma evolution, which means a sudden change of crystallization condition in the magmatic system, i.e. magma eruption (Hui HJ et al., 2011). Moreover, the late-stage minerals (Fe-rich pyroxenes and symplektite) indicate rapidly cooling and low pressure, which also suggests a crystallization condition near the Martian surface. So an eruption scenario would be reasonable to explain the petrography and mineral chemistry of NWA 8656 based on the above discussion.

NWA 8656 is an extrusive rock with subophitic texture. This can be reasonably explained by the cessation of nucleation of late-stage Fe-rich pyroxenes. The euhedral granular texture of early-stage pyroxene cores indicates that they crystallized with nucleation in the base of the Martian crust or the mantle/crust boundary. Then Fe-rich pyroxenes overgrew onto pyroxene cores without nucleation in the Martian surface, rather than crystallizing as fine-grained matrix mineral. Therefore, since NWA 8656 appears as subophitic texture consisting of euhedral pyroxene and maskelynite without fine-grained groundmass, a three-stage episode of NWA 8656 magmatic evolution can be proposed (Figure 5): 1) Mg-rich pyroxenes crystallized with nucleation at depth, forming pyroxene cores; 2) The magma ascended with entrained Mg-rich pyroxene crystals and plagioclase crystallized with nucleation; 3) The final magma erupted as a lava flow and crystallized late-stage mineral phases. Fe-Ti oxides and phosphates crystallized with nucleation; Fe-rich pyroxenes overgrew onto Mg-rich pyroxene cores without nucleation.

4.4 NWA 8656 Represents the Parent Melt Composition

Obviously, NWA 8656 and 8657 are relatively low-Mg compared to those basaltic shergottites that contain cumulus pyroxene crystals, such as Shergotty and Zagami (Figure 6). The origin of the most magnesian pyroxenes in shergottites, cumulus or phenocryst, can be inferred if they are in equilibrium with the bulk rock composition (Kring et al., 2003). The range of equilibrium pyroxene composition is limited to two curves in Figure 6 by calculating the Mg# of pyroxene in equilibrium with the bulk rock compositon using the crystal/melt partition coefficients of Stolper and McSween (1979) and Bédard (2010) ($D^{(FeO/MgO)}_{aug/melt}$ = 0.27 and 0.312). It is notable that element partition coefficients of pyroxene are closely related to the Ca content in pyroxenes (Lundberg et al. 1990; McKay et al. 1986). So only augite can be used in the calculation because pigeonite is low in Ca. The bulk rock Mg# of NWA 8656 is referred to NWA 8657 of Howarth et al. (2018). The measured Mg# of the earliest-formed pyroxene core in NWA 8656 is similar to the calculated equilibrium composition of pyroxene (Figure 6), suggesting that it is in equilibrium with the bulk rock composition. It also implies that these pyroxenes are not of cumulus origin but phenocryst origin. The basaltic shergottites that contain cumulus pyroxene crystals show a higher Mg# of bulk rock composition. So the low Mg# of NWA 8656 also suggests that it contains no or only rare cumulus pyroxenes.

If NWA 8656 represents the parent melt composition, then the REE compositions of the earliest-formed pyroxene cores (the most magnesian pyroxene) should be in equilibrium with the bulk rock REE compositions. So we calculated the REE abundances of the melt in equilibrium with the augite cores (Mg# 69–68) in NWA 8656/8657 using the crystal/melt partition coefficient, $D_{aug\text{-}melt}$ for augite of Wo_{33}, of Mckay et al. (1986). But this approach is unable to estimate accurately the absolute REE abundances of the parent melt because of uncertainties in the values of the absolute partition coefficients. The result shows that the calculated parent melt REE concentrations are almost identical to the bulk rock REE concentrations of NWA 8657 (Figure 7). Consequently, NWA 8656 can represent the parent melt composition and be directly used to analyze the magmatic evolution process.

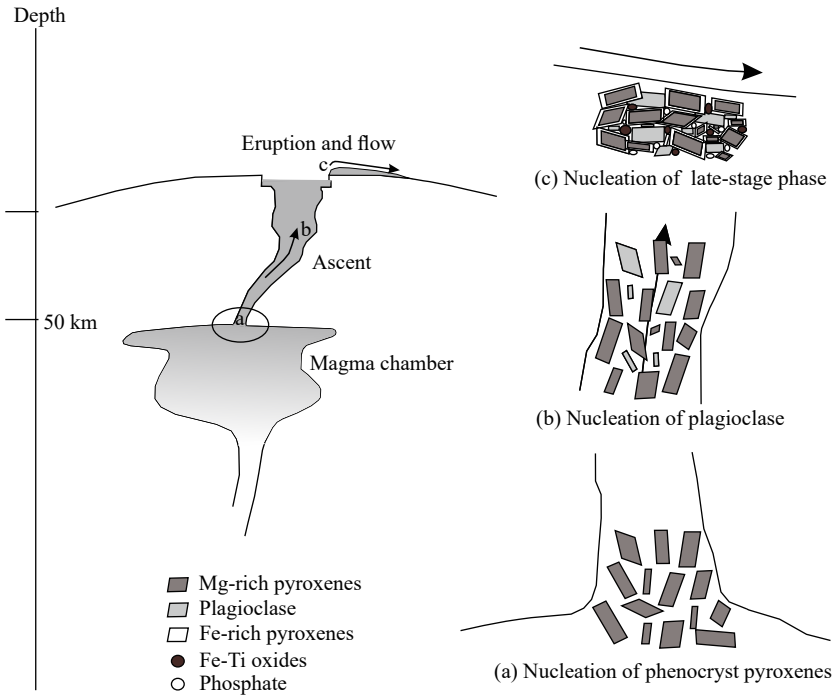

Figure 5. Schematic of a three-stage episode for the petrogenesis of NWA 8656. (a) Mg-rich pyroxenes crystallization at depth with nucleation; (b) The ascent of magma with entrained pyroxene crystals, and plagioclase crystallization with nucleation; (c) The magma eruption onto the surface that formed a lava flow, late-stage mineral phases crystallization, Fe-rich pyroxenes overgrowth onto Mg-rich pyroxenes without nucleation.

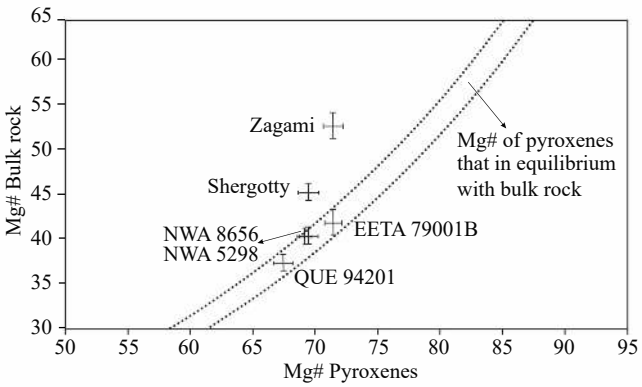

Figure 6. Mg# of measured augite cores and calculated pyroxene composition that is in equilibrium with a melt with their bulk composition. The comparing data come from Hui HJ et al. (2011), McSween et al. (1996).

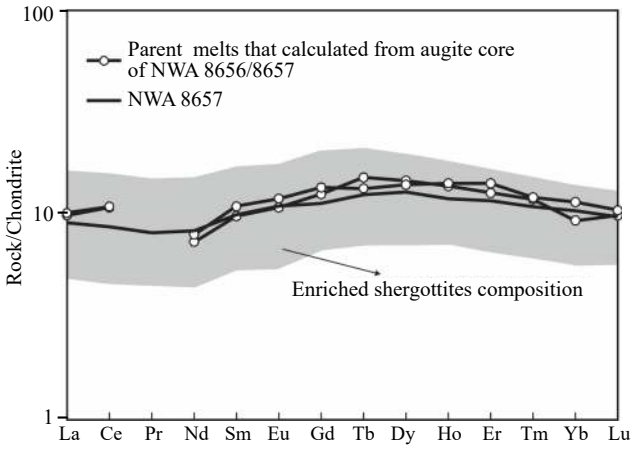

Figure 7. CI chondrite-normalized calculated REE patterns of melts that equilibrated with the cores of augite of NWA 8656/8657 and the bulk rock REE patterns of NWA 8657 and enriched shergottites suite are used for reference. Other enriched shergottites data come from Howarth (2017), Stolper and McSween (1979), Taylor (2002), Zipfel (2000).

4.5 Crustal Assimilation

Many previous studies have reported that the ITE-enriched geochemical characteristics of shergottites are attributed to the assimilation of the enriched Martian crust, which also suggests an open crystallization system of enriched shergottites. However, most enriched shergottites are crystallized in a closed-system, such as NWA 856 and NWA 5298 (Hui HJ et al., 2011; Ferdous et al., 2017). Therefore, we wished to determine whether NWA 8656 formation is consistent with progressive crystallization in a closed-system.

First, a fractional crystallization model was chosen, because of the extensive zoning of pyroxenes in NWA 8656. The bulk rock REE composition for NWA 8657 is used as the initial parent melt composition, C_o. Because REE partition coefficients of pyroxene are closely related to the content of Ca in pyroxenes, we have chosen $D_{aug\text{-}melt}$ for augite of Wo_{33} and $D_{pgt\text{-}melt}$ for pigeonite of Wo_{13} (Lundberg et al., 1990; McKay et al., 1986). Partition coefficients for plagioclase are referred to Lundberg et al. (1990). Based on the above discussion, pyroxene cores crystallize in the first step, assuming

the degree of fractional crystallization is F=0.9, C_s =aug core + pgt core (1:1) and the partition coefficient is D_i=$D_{aug\text{-}melt}$×0.5 +$D_{aug\text{-}melt}$× 0.5. Assuming the degree of fractional crystallization of plagioclase is F=0.5, C_s =aug core + pgt core (1:1) and the partition coefficient is D_i=$D_{aug\text{-}melt}$×0.5 +$D_{aug\text{-}melt}$×0.5. The crystallization of plagioclase is followed by pyroxene rims, so assuming that the degree of fractional crystallization of augite rim is F=0.4, C_s =aug core + pgt core + pl (1:1:1) and the partition coefficient is D_i=$D_{aug\text{-}melt}$×0.33+ $D_{aug\text{-}melt}$×0.33+$D_{pl\text{-}melt}$×0.33. All the above assumptions of the degree of fractional crystallization and mineral proportion of C_s have referred to the MELTS simulation of other similar basaltic shergottites, e.g. Shergotty and NWA 856 (Stolper and McSween, 1979; Ferdous et al., 2017). The results show that the REE compositions of augite core, pigeonite core, and augite rim can be fit with a fractional crystallization model at F=0.9 and 0.4, while plagioclase can be fit at F =0.5 (Figure 8). Because we cannot accurately assume the proportion of pyroxene and plagioclase in C_S for F=0.4, the Eu anomaly in augite rim is not consistent with the measured compositions. Additionally, because of a lower content of HREE in plagioclase and uncertainty of measurement, some calculated HREE compositions are not consistent with the measured compositions.

In general, the REE compositions of early-stage phases (pyroxene cores), and late-stage phases (plagioclase and pyroxene rims) for both NWA 8656 and 8657 could be reproduced by the progressive fractional crystallization model without any exogenous component. Therefore, NWA 8656/8657 appear to have crystallized from an enriched magma in a closed-system. And the ITE-enriched signature of NWA 8656 cannot be attributed to crustal assimilation.

4.6 Fractional Crystallization

The low Mg# of basaltic shergottites (40–30) suggests that they are not parent magmas but evolving magmas, and this differentiation could be caused by fractional crystallization. The existence of cumulus minerals in most shergottites also implies fractional crystallization processes; for example, Shergotty contains 28% cumulus pyroxenes; NWA 1068 contains 22% cumulus olivine, and Los Angeles contains significant cumulus plagioclase. Hence, basaltic shergottites are likely to have been evolving magmas that differentiated by crystal fractionation of olivine, pyroxene, or plagioclase. The variations of major element composition result chiefly from varying degrees of fractional crystallization (Shearer et al., 2013; Symes et al., 2008; Treiman and Filiberto, 2015; Usui et al., 2008). A parent magma with REE abundances like NWA 1068 (Mg# = 59) could produce an evolving melt with REE abundances like those of Los Angeles by 30% crystal fractionation (Treiman and Filiberto., 2015). NWA 8656 is more primitive (Mg# = 41) than Los Angeles (Mg# = 30, Warren et al., 2004), which indicates a small amount of crystal fractionation of NWA 8656 parent magma. NWA 1068 is an olivine-phyric shergottite that shows similar REE pattern to basaltic shergottites, such as Shergotty and NWA 8656, suggesting a close connection between NWA 1068 and NWA 8656. Because NWA 1068 is more primitive than NWA 8656, we assumed that the parent magma of NWA 8656 has REE abundances similar to NWA 1068 (minus 22% cumulus olivine crystals). It is notable that NWA 1068 cannot be the real parent magma of NWA

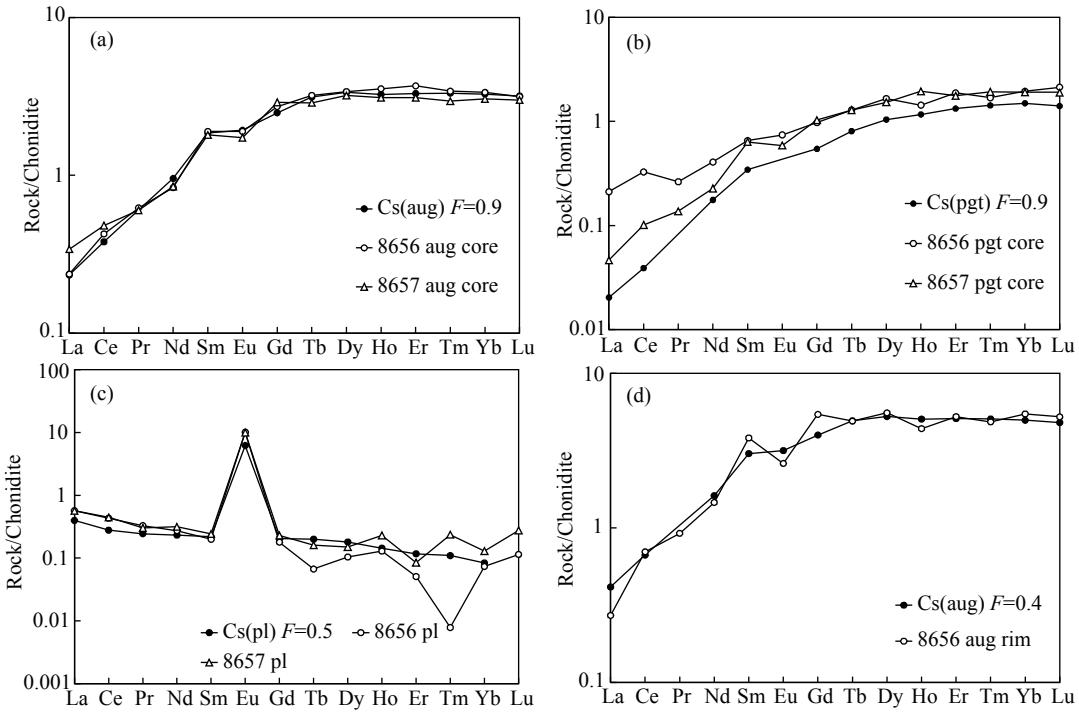

Figure 8. Calculated REE compositions of pyroxenes and plagioclase in NWA 8656/8657. (a) Augite core; (b) Pigeonite core; (c) Plagioclase; (d) Augite rim. We calculated the different mineral compositions in different degrees of fractional crystallization based on the formula, $C_s = D_i \times C_o^i \times F^{D_i-1}$. The compositions of NWA 8657 (Howarth et al., 2018) are used as C_o, and the D_i is calculated by the REE partition coefficients of C_S -pyroxenes and plagioclase and the proportions of them for different degrees of fractional crystallization F.

8656. Then, we calculated the degree of differentiation by Raleigh fractionation. The REE composition of NWA 1068 is C_o, NWA 8656 is C_l (refer to NWA 8657 composition) and $F = C_o/C_l$. Th, Rb and Ta were used for calculation because these are highly incompatible elements and the partition coefficients $D_{\text{mineral-melt}}$ almost equal to 0 for nearly all minerals (olivine, pyroxenes, and plagioclase). The result shows that a parent magma with REE abundances similar to those of NWA 1068 (minus 22% cumulus olivine crystal) could produce the parent melt of NWA 8656 by approximately 7–9 % crystal fractionation.

4.7 The Mantle Source of Enriched Shergottites

The geochemical characteristics of NWA 8656 suggest a closed magmatic system without Martian crustal assimilation. Moreover, the low degree fractional crystallization of NWA 8656 parent melt suggests that it is a mantle-origin igneous rock. Consequently, the ITE-enriched signature of NWA 8656 is inherited from the enriched mantle source rather than caused by crustal assimilation.

HREE are stable in late-stage geologic processes, such as fractional crystallization and terrestrial alteration; therefore they can be used to estimate the partial melting degree of mantle cumulate. The depleted Martian mantle (DMM) is composed of olivine, clinopyroxene, orthopyroxene, and garnet, and partial melting of this mantle cumulate can yield a melt with trace element and isotope compositions characteristic of depleted shergottites (Borg and Draper, 2003; Debaillie et al., 2008; Shimoda et al., 2005). A low degree partial melting can yield an ITE-enriched melt, so we calculated the REE composition of the melt that experienced low degree partial melting of depleted Martian mantle. The result shows that the calculated melt composition is lower than that of NWA 8656, even only 1% partial melting of depleted Martian mantle (Figure 9), and such a low degree of partial melting is totally unreasonable. Although low degree partial melting of depleted mantle source can produce an ITE-enriched magma, partial melting of depleted Martian mantle would not directly yield ITE-enriched magmas similar to the enriched shergottites parent magma. So the enriched and depleted shergottites are derived from distinct mantle sources, and the mineralogical composition of the mantle source of enriched shergottites is different from that of depleted shergottites.

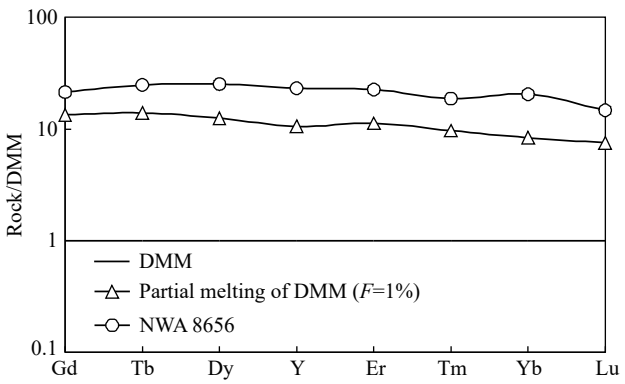

Figure 9. Depleted Martian mantle normalized HREE diagram for calculated abundances of parent magma that experienced low degree partial melting of the depleted Martian mantle. The composition and mineralogical model of DMM come from Borg and Draper (2003), the data of NWA 8656 refer to NWA 8657 of Howarth (2017).

The enriched mantle source would be in the shallow Martian upper mantle (Shearer et al., 2013; Symes et al., 2008; Debaille et al., 2008), and ilmenite may exist in the shallow Martian upper mantle (Borg and Draper, 2003), so the upper Martian mantle cumulate may contain ilmenite. This assumption is consistent with the enrichment in Zr and Hf found in enriched shergottites (Figure 10), and this enrichment could be attributed to the presence of ilmenite, enriched in Zr and Hf, in the mantle source of enriched shergottites. It is notable that both depleted and enriched shergottites contain minor amounts of ilmenite (~2 %), but only enriched shergottites show enrichment in Zr and Hf, so this enrichment is associated with the existence of ilmenite in the mantle source, rather than the ilmenite mineral in the shergottites. Consequently, enriched shergottites would be derived from the enriched mantle source that may contain ilmenite.

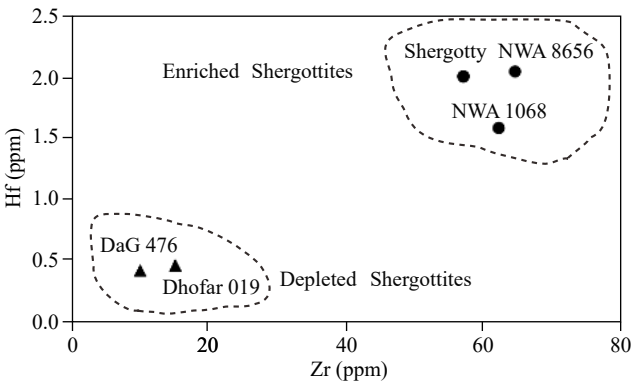

Figure 10. Zr and Hf contents in shergottites. The enriched shergottites show enrichment in Zr and Hf. Other shergottite data come from Filiberto (2010), Stolper and McSween (1979), Taylor (2002), Zipfel (2000), the data of NWA 8656 refer to NWA 8657 of Howarth (2017).

5. Conclusions and Summary

Northwest Africa 8656 is an enriched basaltic shergottite that can represent the parent melt composition. The REE abundances of pyroxenes and plagioclase can be successfully reproduced by progressive crystallization without any exogenous component. So we infer that NWA 8656 crystallized from an enriched melt in a closed system. Consequently, the ITE-enriched signature of NWA 8656 is inherited from an enriched mantle source, rather than caused by Martian crustal assimilation. Partial melting of the depleted Martian mantle cannot directly yield the parent magmas of enriched shergottites, so the enriched and depleted shergottites are derived from distinct mantle sources, and the mantle source of enriched shergottites may contain ilmenite.

Acknowledgements

For their help with the SEM, EMP and LA-ICP-MS, we thank all laboratory workers at the State Key Laboratory of Geological Processes and Mineral Resources, China University of Geosciences,

Wuhan and Wuhan University of Technology . We also greatly appreciate the helpful comments by editor Q Huang and S Hu, and reviewers S Hu and H Hui.

References

Anand, M., Taylor, L. A., Floss, C., Neal, C. R., Terada, K., and Tanikawa, S. (2006). Petrology and geochemistry of LaPaz Icefield 02205: A new unique low-Ti mare-basalt meteorite. *Geochim. Cosmochim. Acta*, *70*(1), 246–264. https://doi.org/10.1016/j.gca.2005.08.018

Aramovich, C. J., Herd, C. D. K., and Papike, J. J. (2002). Symplectites derived from metastable phases in Martian basaltic meteorites. *Am. Miner*, *87*(10), 1351–1359. https://doi.org/10.2138/am-2002-1010

Barrat, J. A., Gillet, P. H., Sautter, V., Jambon, A., Javoy, M., Göpel, C., Lesourd, M., Keller, F., and Petit, E. (2002). Petrology and chemistry of the basaltic shergottite North West Africa 480. *Meteorit. Planet. Sci.*, *37*(4), 487–499. https://doi.org/10.1111/j.1945-5100.2002.tb00835.x

Bédard, J. H. (2010). Parameterization of The Fe-Mg exchange coefficient (Kd) between clinopyroxene and silicate melts. *Chem. Geol.*, *274*(3–4), 169–176. https://doi.org/10.1016/j.chemgeo.2010.04.003

Blichert-Tolt, J., Gleason, J. D., Télouk, P., and Albarède, F. (1999). The Lu–Hf isotope geochemistry of shergottites and the evolution of the Martian mantle-crust system. *Earth Planet. Sci. Lett.*, *173*(1–2), 25–39. https://doi.org/10.1016/S0012-821X(99)00222-8

Borg, L. E., Nyquist, L. E., Taylor, L. A., Wiesmann, H., and Shih, C. Y. (1997). Constraints on Martian differentiation processes from Rb–Sr and Sm–Nd isotopic analyses of the basaltic shergottite QUE 94201. *Geochim. Cosmochim. Acta*, *61*(22), 4915–4931. https://doi.org/10.1016/S0016-7037(97)00276-7

Borg, L. E., and Draper, D. A. (2003). A petrogenetic model for the origin and compositional variation of the Martian basaltic meteorites. *Meteorit. Planet. Sci.*, *38*(12), 1713–1731. https://doi.org/10.1111/j.1945-5100.2003.tb00011.x

Bouvier, A., Blichert-Tolt, J., Vervoort, J. D., Gillet, P., and Albarède, F. (2008a). The case for old basaltic shergottites. *Earth Planet. Sci. Lett.*, *266*(1–2), 105–124. https://doi.org/10.1016/j.epsl.2007.11.006

Bouvier, A., Vervoort, J. D., and Patchett, P. J. (2008b). The Lu–Hf and Sm–Nd isotopic composition of CHUR: constraints from unequilibrated chondrites and implications for the bulk composition of terrestrial planets. *Earth Planet. Sci. Lett.*, *273*(1–2), 48–57. https://doi.org/10.1016/j.epsl.2008.06.010

Brandon, A. D., Puchtel, I. S., Walker, R. J., Day, J. M. D., Irving, A. J., and Taylor, L. A. (2012). Evolution of the Martian mantle inferred from the ^{187}Re-^{187}Os isotope and highly siderophile element abundance systematics of Shergottite meteorites. *Geochim. Cosmochim. Acta*, *76*, 206–235. https://doi.org/10.1016/j.gca.2011.09.047

Bridges, J. C., and Warren, P. H. (2006). The SNC meteorites: basaltic igneous processes on Mars. *J. Geol. Soc.*, *163*(2), 229–251. https://doi.org/10.1144/0016-764904-501

Chen, L., Liu, Y. S., Hu, Z. C., Gao, S., Zong, K. Q., and Chen, H. H. (2011). Accurate determinations of fifty-four major and trace elements in carbonate by LA-ICP-MS using normalization strategy of bulk components as 100%. *Chem. Geol.*, *284*(3–4), 283–295. https://doi.org/10.1016/j.chemgeo.2011.03.007

Crozaz, G., Floss, C., and Wadhwa, M. (2003). Chemical alteration and REE mobilization in meteorites from hot and cold deserts. *Geochim. Cosmochim. Acta*, *67*(24), 4727–4741. https://doi.org/10.1016/j.gca.2003.08.008

Debaille, V., Brandon, A. D., Yin, Q. Z., and Jacobsen, B. (2007). Coupled ^{142}Nd - ^{143}Nd evidence for a protracted magma ocean in Mars. *Nature*, *450*(7169), 525–528. https://doi.org/10.1038/nature06317

Debaille, V., Yin, Q. Z., Brandon, A. D., and Jacobsen, B. (2008). Martian Mantle mineralogy investigated by the ^{176}Lu-^{176}Hf and ^{147}Sm-^{143}Nd systematics of shergottites. *Earth Planet. Sci. Lett.*, *269*(1–2), 186–199. https://doi.org/10.1016/j.epsl.2008.02.008

Ferdous, J., Brandon, A. D., Peslier, A. H., and Pirotte, Z. (2017). Evaluating crustal contributions to enriched shergottites from the petrology, trace elements, and Rb-Sr and Sm-Nd isotope systematics of Northwest Africa 856. *Geochim. Cosmochim. Acta*, *211*, 280–306. https://doi.org/10.1016/j.gca.2017.05.032

Filiberto, J., Musselwhite, D. S., Gross, J., Burgess, K., Le, L., and Treiman, A. H. (2010). Experimental petrology, crystallization history, and parental magma characteristics of olivine-phyric shergottite NWA 1068: Implications for the petrogenesis of "enriched" olivine-phyric shergottites. *Meteorit. Planet. Sci.*, *45*(8), 1258–1270. https://doi.org/10.1111/j.1945-5100.2010.01080.x

Filiberto, J., Gross, J., Trela, J., and Ferre, E. C. (2014). Gabbroic shergottite Northwest Africa 6963: an intrusive sample of Mars. *Am. Mineral.*, *99*(4), 601–606. https://doi.org/10.2138/am.2014.4638

Fritz, J., Artemieva, N., and Greshake, A. (2005). Ejection of Martian meteorites. *Meteorit. Planet. Sci.*, *40*(9–10), 1393–1411. https://doi.org/10.1111/j.1945-5100.2005.tb00409.x

Ghiorso, M. S., and Sack, O. (1991). Fe-Ti oxide geothermometry: Thermodynamic formulation and the estimation of intensive variables in silicic magmas. *Contrib. Mineral. Petrol.*, *108*(4), 485–510. https://doi.org/10.1007/BF00303452

Ghiorso, M. S., and Evans, B. W. (2008). Thermodynamics of rhombohedral oxide solid solutions and a revision of the Fe-Ti two-oxide geothermometer and oxygen-barometer. *Am. J. Sci.*, *308*(9), 957–1039. https://doi.org/10.2475/09.2008.01

Goodrich, C. A. (2002). Olivine-phyric Martian basalts: a new type of shergottite. *Meteorit. Planet. Sci.*, *37*(S12), B31–B34. https://doi.org/10.1111/j.1945-5100.2002.tb00901.x

Goodrich, C. A. (2003). Petrogenesis of olivine-phyric shergottites Sayh Al Uhaymir 005 and elephant moraine A79001 lithology A. *Geochim. Cosmochim. Acta*, *67*(19), 3735–3772. https://doi.org/10.1016/S0016-7037(03)00171-6

He, Q., Xiao, L., Balta, J. B., Baziotis, I. P., Hsu, W., and Guan, Y. B. (2015). Petrography and geochemistry of the enriched basaltic shergottite Northwest Africa 2975. *Meteorit. Planet. Sci.*, *50*(12), 2024–2044. https://doi.org/10.1111/maps.12571

Herd, C. D. K., Papike, J. J., and Brearley, A. J. (2001). Oxygen fugacity of Martian basalts from electron microprobe oxygen and TEM-EELS analyses of Fe-Ti oxides. *Am. Miner.*, *86*(9), 1015–1024. https://doi.org/10.2138/am-2001-8-908

Herd, C. D. K., Borg, L. E., Jones, J. H., and Papike, J. J. (2002). Oxygen fugacity and geochemical variations in the Martian basalts: Implications for Martian basalt petrogenesis and the oxidation state of the upper mantle of Mars. *Geochim. Cosmochim. Acta*, *66*(11), 2025–2036. https://doi.org/10.1016/S0016-7037(02)00828-1

Herd, C. D. K. (2006). Insights into the redox history of the NWA 1068/1110 Martian basalt from mineral equilibria and vanadium oxybarometry. *Am. Miner.*, *91*(10), 1616–1627. https://doi.org/10.2138/am.2006.2104

Howarth, G. H., Udry, A., and Day, J. M. D. (2018). Petrogenesis of basaltic shergottite Northwest Africa 8657: Implications for fO_2 correlations and element redistribution during shock melting in shergottites. *Meteorit. Planet. Sci.*, *53*(2), 249–267. https://doi.org/10.1111/maps.12999

Hui, H. J., Peslier, A. H., Lapen, T. J., Shafer, J. T., Brandon, A. D., and Irving, A. J. (2011). Petrogenesis of basaltic shergottite Northwest Africa 5298: closed-system crystallization of an oxidized mafic melt. *Meteorit. Planet. Sci.*, *46*(9), 1313–1328. https://doi.org/10.1111/j.1945-5100.2011.01231.x

Jones, J. H. (1986). A discussion of isotopic systematics and mineral zoning in the shergottites: Evidence for a 180 m.y. igneous crystallization age. *Geochim. Cosmochim. Acta*, *50*(6), 969–977. https://doi.org/10.1016/0016-7037(86)90377-7

Kring, D. A., Gleason, J. D., Swindle, T. D., Nishiizumi, K., Caffee, M. W., Hill, D. H., Jull, A. J. T., and Boynton, W. V. (2003). Composition of the first bulk melt sample from a volcanic region of Mars: Queen Alexandra Range 94201. *Meteorit. Planet. Sci.*, *38*(12), 1833–1848. https://doi.org/10.1111/j.1945-5100.2003.tb00018.x

Lentz, R. C. F., and McSween, Jr. H. Y. (2000). Crystallization of the basaltic shergottites: Insights from crystal size distribution (CSD) analysis of pyroxenes. *Meteorit. Planet. Sci.*, *35*(5), 919–927. https://doi.org/10.1111/j.1945-5100.2000.tb01481.x

Lindsley, D. H., and Burnham, C. W. (1970). Pyroxferroite: Stability and X-ray crystallography of synthetic $Ca_{0.15}Fe_{0.85}SiO_3$ pyroxenoid. *Science*, *168*(3929), 364–367. https://doi.org/10.1126/science.168.3929.364

Lindsley, D. H., and Andersen, D. J. (1983). A two-pyroxene thermometer. *J. Geophys. Res.*, *88*(S02), A887–A906. https://doi.org/10.1029/JB088iS02p0A887

Lindsley, D. H. (1983). Pyroxene thermometry. *Am. Min.*, *68*(5–6), 477–493.

Liu, Y. S., Hu, Z. C., Gao, S., Günther, D., Xu, J., Gao, C. G., and Chen, H. H. (2008). *In situ* analysis of major and trace elements of anhydrous minerals by LA-

ICP-MS without applying an internal standard. *Chem. Geol.*, *257*(1–2), 34–43. https://doi.org/10.1016/j.chemgeo.2008.08.004

Lodders, K. (1998). A survey of shergottite, nakhlite and chassigny meteorites whole-rock compositions. *Meteorit. Planet. Sci.*, *33*(S4), A183–A190. https://doi.org/10.1111/j.1945-5100.1998.tb01331.x

Lu, F., Taylor, L. A., and Jin, Y. (1989). Basalts and gabbros from Mare Crisium-Evidence for extreme fractional crystallization. In *Proceedings of the 19th Lunar and Planetary Science Conference* (pp. 199–207). Houston, TX: Cambridge University Press/Lunar and Planetary Institute.

Lundberg, L. L., Crozaz, G., McKay, G., and Zinner, E. (1988). Rare earth element carriers in the Shergotty meteorite and implications for its chronology. *Geochim. Cosmochim. Acta*, *52*(8), 2147–2163. https://doi.org/10.1016/0016-7037(88)90194-9

Lundberg, L. L., Crozaz, G., and McSween, H. Y. (1990). Rare earth elements in minerals of the ALHA77005 shergottite and implications for its parent magma and crystallization history. *Geochim. Cosmochim. Acta*, *54*(9), 2535–2547. https://doi.org/10.1016/0016-7037(90)90240-L

McKay, G., Wagstaff, J., and Yang, S. R. (1986). Clinopyroxene REE distribution coefficients for shergottites: The REE content of the Shergotty melt. *Geochim. Cosmochim. Acta*, *50*(6), 927–937. https://doi.org/10.1016/0016-7037(86)90374-1

McSween, Jr. H. Y. (1994). What we have learned about Mars from SNC meteorites. *Meteoritics*, *29*(6), 757–779. https://doi.org/10.1111/j.1945-5100.1994.tb01092.x

McSween, Jr. H. Y., Eisenhour, D. D., Taylor, L. A., Wadhwa, M., and Crozaz, G. (1996). QUE94201 shergottite: crystallization of a Martian basaltic magma. *Geochim. Cosmochim. Acta*, *60*(22), 4563–4569. https://doi.org/10.1016/S0016-7037(96)00265-7

McSween, H. Y., Treiman, A. H. (1998). Martian meteorites. *Rev Mineral*, *36*, 6-1–6-53.

Mikouchi, T., Miyamoto, M., and McKay, G. A. (1999). The role of undercooling in producing igneous zoning trends in pyroxenes and maskelynites among basaltic Martian meteorites. *Earth Planet. Sci. Lett.*, *173*(3), 235–256. https://doi.org/10.1016/S0012-821X(99)00188-0

Nyquist, L. E., Bansal, B. M., Wiesmann, H., and Shih, C. Y. (1995). "Martians" young and old: Zagami and ALH 84001. In *Proceedings of the 26th Lunar and Planetary Science Conference* (pp. 1065–1066). Houston, TX: Cambridge University Press/Lunar and Planetary Institute.

Nyquist, L. E., Bogard, D. D., Shih, C. Y., Greshake, A., Stöffler, D., and Eugster, O. (2001). Ages and geologic histories of Martian meteorites. *Space Sci. Rev.*, *96*(1–4), 105–164. https://doi.org/10.1023/A:1011993105172

Papike, J. J., Karner, J. M., Shearer, C. K., and Burger, P. V. (2009). Silicate mineralogy of Martian meteorites. *Geochim. Cosmochim. Acta*, *73*(24), 7443–7485. https://doi.org/10.1016/j.gca.2009.09.008

Patzer, A., and McSween, Jr. H. Y. (2012). Ordinary (mesostasis) and not-so-ordinary (symplectites) late-stage assemblages in howardites. *Meteorit. Planet. Sci.*, *47*(9), 1475–1490. https://doi.org/10.1111/j.1945-5100.2012.01408.x

Rost, D., Stephan, T., Greshake, A., Fritz, J., Weber, I., and Jessberger, E. K., Stöffler, D. (2009). A combined ToF- SIMS and EMP/SEM study of a three-phase symplectite in the Los Angeles basaltic shergottite. *Meteorit. Planet. Sci.*, *44*(8), 1225–1237. https://doi.org/10.1111/j.1945-5100.2009.tb01219.x

Shafer, J. T., Brandon, A. D., Lapen, T. J., Righter, M., Peslier, A. H., and Beard, B. L. (2010). Trace element systematics and ^{147}Sm-^{143}Nd and ^{176}Lu-^{176}Hf ages of Larkman Nunatak 06319: closed-system fractional crystallization of an enriched shergottite magma. *Geochim. Cosmochim. Acta*, *74*(24), 7307–7328. https://doi.org/10.1016/j.gca.2010.09.009

Shearer, C. K., Aaron, P. M., Burger, P. V., Guan, Y., Bell, A. S., and Papike, J. J. (2013). Petrogenetic linkages among fO_2, isotopic enrichments-depletions and crystallization history in Martian basalts. Evidence from the distribution of phosphorus in olivine megacrysts. *Geochim. Cosmochim. Acta*, *120*, 17–38. https://doi.org/10.1016/j.gca.2013.06.034

Shih, C. Y., Nyquist, L. E., Bogard, D. D., McKay, G. A., Wooden, J. L., Bansal, B. M., and Wiesmann, H. (1982). Chronology and petrogenesis of young achondrites, Shergotty, Zagami, and ALHA77005: late magmatism on a geologically active planet. *Geochim. Cosmochim. Acta*, *46*(11), 2323–2344. https://doi.org/10.1016/0016-7037(82)90205-8

Shih, C. Y., Nyquist, L. E., Wiesmann, H., and Barrat, J. A. (2003). Age and petrogenesis of picritic shergottite NWA 1068: Sm-Nd and Rb-Sr isotopic studies. In *Proceedings of the 34th Annual Lunar and Planetary Science Conference*. Houston, TX: NASA Johnson Space Center.

Shimoda, G., Ikeda, Y., Kita, N. T., Morishita, Y., and Imae, N. (2005). Two-stage plume melting: A possible mechanism for the origin of Martian magmatism. *Earth Planet. Sci. Lett.*, *235*(3–4), 469–479. https://doi.org/10.1016/j.epsl.2005.05.005

Stöffler, D., Ostertag, R., Jammes, C., Pfannschmidt, G., Gupta, P. R. S., Simon, S. B., Papike, J. J., and Beauchamp, R. H. (1986). Shock metamorphism and petrography of the Shergotty achondrite. *Geochim. Cosmochim. Acta*, *50*(6), 889–903. https://doi.org/10.1016/0016-7037(86)90371-6

Stolper, E., and McSween, Jr. H. Y. (1979). Petrology and origin of the shergottite meteorites. *Geochim. Cosmochim. Acta*, *43*(9), 1475–1498. https://doi.org/10.1016/0016-7037(79)90142-X

Sun, S. S., and McDonough, W. F. (1989). Chemical and isotopic systematics of oceanic basalts: Implications for mantle composition and processes. In A. D. Saunders and M. J. Norry (Eds.), *Magmatism in the Ocean Basins* (pp. 313–345). Geological Society, London, Special Publications.

Symes, S. J. K., Borg, L. E., Shearer, C. K., and Irving, A. J. (2008). The age of the Martian meteorite Northwest Africa 1195 and the differentiation history of the shergottites. *Geochim. Cosmochim. Acta*, *72*(6), 1696–1710. https://doi.org/10.1016/j.gca.2007.12.022

Taylor, L. A., Nazarov, M. A., Ivanova, M. A., Patchen, A., Clayton, R. N., and Mayeda, T. K. (2000). Petrology of the Dhofar 019 shergottite. *Meteorit. Planet. Sci.*, *35*(5), 155–159.

Treiman, A. H. (1996). The perils of partition: Difficulties in retrieving magma compositions from chemically equilibrated basaltic meteorites. *Geochim. Cosmochim. Acta*, *60*(1), 147–155. https://doi.org/10.1016/0016-7037(95)00393-2

Treiman, A. H., and Filiberto, J. (2015). Geochemical diversity of shergottite basalts: Mixing and fractionation, and their relation to Mars surface basalts. *Meteorit. Planet. Sci.*, *50*(4), 632–648. https://doi.org/10.1111/maps.12363

Udry, A., Howarth, G. H., Lapen, T. J., and Righter, M. (2017). Petrogenesis of the NWA 7320 enriched Martian gabbroic shergottite: Insight into the Martian crust. *Geochim. Cosmochim. Acta.*, *204*, 1–18. https://doi.org/10.1016/j.gca.2017.01.032

Usui, T., McSween, Jr. H. Y., and Floss, C. (2008). Petrogenesis of olivine-phyric shergottite Yamato 980459, revisited. *Geochim. Cosmochim. Acta*, *72*(6), 1711–1730. https://doi.org/10.1016/j.gca.2008.01.011

Wadhwa, M., McSween, Jr. H. Y., and Crozaz, G. (1994). Petrogenesis of shergottite meteorites inferred from minor and trace element microdistributions. *Geochim. Cosmochim. Acta*, *58*(19), 4213–4229. https://doi.org/10.1016/0016-7037(94)90274-7

Wadhwa, M. (2001). Redox state of Mars' upper mantle and crust from Eu anomalies in shergottite pyroxenes. *Science*, *291*(5508), 1527–1530. https://doi.org/10.1126/science.1057594

Warren, P. H., Greenwood, J. P., and Rubin, A. E. (2004). Los Angeles: a tale of two stones. *Meteorit. Planet. Sci.*, *39*(1), 137–156. https://doi.org/10.1111/j.1945-5100.2004.tb00054.x

Warren, P. H., and Bridges, J. C. (2005). Geochemical subclassification of shergottites and the crustal assimilation model. In *Proceedings of the 36th Lunar and Planetary Science Conference*. League City, Texas: Cambridge University Press/Lunar and Planetary Institute.

Wieczorek, M. A. and Zuber, M. T. (2004). Thickness of the Martian crust: Improved constraints from geoid-to-topography ratios. *J. Geophys. Res.*, *109*(E1), E01009. https://doi.org/10.1029/2003JE002153

Zipfel, J., Scherer, P., Spettel, B., Dreibus, G., Schultz, L. (2000). Petrology and chemistry of the new shergottite Dar al Gani 476. *Meteorit. Planet. Sci.*, *35*(1), 95–106. https://doi.org/10.1111/j.1945-5100.2000.tb01977.x